

Polarization of Rayleigh Scattered Ly α in Active Galactic Nuclei

Seok-Jun Chang,^{1*} Hee-Won Lee^{1†} and Yujin Yang^{2,3}

¹ *Department of Physics and Astronomy, Sejong University, Seoul, Korea*

² *Korea Astronomy and Space Science Institute, Daejeon, Korea*

³ *Korea University of Science and Technology (UST), 217 Gajeong-ro Yuseong-gu, Daejeon 34113, Korea*

Accepted XXX. Received YYY; in original form ZZZ

ABSTRACT

The unification scheme of active galactic nuclei (AGNs) invokes an optically thick molecular torus component hiding the broad emission line region. Assuming the presence of a thick neutral component in the molecular torus characterized by a H I column density $> 10^{22} \text{ cm}^{-2}$, we propose that far UV radiation around Ly α can be significantly polarized through Rayleigh scattering. Adopting a Monte Carlo technique we compute polarization of Rayleigh scattered radiation near Ly α in a thick neutral region in the shape of a slab and a cylindrical shell. It is found that radiation near Ly α Rayleigh reflected from a very thick slab can be significantly polarized in a fairly large range of wavelength $\Delta\lambda \sim 50 \text{ \AA}$ exhibiting a flux profile similar to the incident one. Rayleigh transmitted radiation in a slab is characterized by the central dip with a complicated polarization behavior. The optically thick part near Ly α center is polarized in the direction perpendicular to the slab normal, which is in contrast to weakly polarized wing parts in the direction parallel to the slab normal. A similar polarization flip phenomenon is also found in the case of a tall cylindrical shell, in which the spatial diffusion along the vertical direction near the inner cylinder wall for core photons leads to a tendency of the electric field aligned to the direction perpendicular to the vertical axis. Observational implications are briefly discussed including spectropolarimetry of the quasar PG 1630+377 by Koratkar et al. in 1990 where Ly α is strongly polarized with no other emission lines polarized.

Key words: polarization – scattering – radiative transfer – quasars: general

1 INTRODUCTION

The spectra of active galactic nuclei (AGNs) are characterized by a nonthermal continuum with prominent emission lines. A huge range of ionization is apparent in the emission line spectra encompassing low ionization species such as Mg II λ 2800 and high ionization lines like O VI λ 1034. AGNs are powered by the accretion process around a supermassive black hole forming a geometrically thin but optically thick disk (Blandford et al. 1990). The emission lines are classified according to their widths where broad lines exhibit a typical width of 10^4 km s^{-1} and narrow emission lines show an order of magnitude smaller width of 500 km s^{-1} .

AGNs are usually classified into two types according to the widths of emission lines. Type 1 AGNs show both broad and narrow emission lines whereas type 2 AGNs exhibit only narrow emission lines. According to unification models of

AGNs all AGNs possess a highly thick molecular torus outside the broad emission line region (e.g. Netzer 2015). In these models, the two types of AGNs are interpreted as an orientation effect toward the observer’s line of sight. Type 1 AGNs are those viewed by the observers with the line of sight near the polar direction whereas to the observers near the equatorial direction AGNs are classified as Type 2.

Spectropolarimetry is an important tool in testing the unification models (e.g. Antonucci 1993). In the case of the prototypical Seyfert 2 galaxy NGC 1068, Antonucci & Miller (1985) found the broad H β emission in the polarized flux spectrum (see also e.g. Miller & Goodrich 1990, Tran et al. 1999). They interpreted this broad H β by assuming the presence of an electron scattering medium in the polar direction that reveals the broad emission line region through Thomson scattering.

Another important test of the unification models is provided by X-ray observations, which reveal that the hardness ratio tends to be systematically higher for type 2 AGNs than type 1 AGNs. In particular, type 2 AGNs typically show se-

* E-mail: csj607@gmail.com

† E-mail: hwlee@sejong.ac.kr

vere extinction in the soft X-ray region, indicating the presence of an absorbing component with hydrogen column density of the order of $N_H \sim 10^{23} \text{ cm}^{-2}$ (e.g. Ricci et al. 2014). Hard X-ray observations of AGNs also show that Compton thick material with column densities $> 10^{24} \text{ cm}^{-2}$ may obscure the AGN engines. Compton scattering from high column components is proposed to be an important contributor to the cosmic X-ray background that is characterized by a broad bump at $\sim 30 \text{ keV}$ (e.g. see Comastri et al. 2015 and Magdziarz et al. 1995). However, the existence and detailed physical conditions of the molecular torus component are only poorly constrained.

As pointed out by Chang et al. (2015), a significant amount of neutral hydrogen that may exist in the hypothetical molecular torus can act as a Rayleigh and Raman scattering medium. The cross section for Rayleigh scattering increases sharply near $\text{Ly}\alpha$ due to resonance. This implies that far UV radiation near $\text{Ly}\alpha$ can be strongly polarized due to Rayleigh scattering depending on the covering factor and the H I column density of the molecular torus. This leads to an interesting possibility of polarized $\text{Ly}\alpha$ to put meaningful constraints on the unification models of AGNs.

Recent detections of polarized $\text{Ly}\alpha$ emission from a giant $\text{Ly}\alpha$ nebula opens a new window to probe the physical environment of the intergalactic medium illuminated by starbursting galaxies and active galactic nuclei in the early universe. $\text{Ly}\alpha$ nebulae, or “blobs,” are rare, extended sources at $z = 2\text{--}6$ with typical $\text{Ly}\alpha$ sizes of $10''$ ($\sim 100 \text{ kpc}$) and line luminosities of $L_{\text{Ly}\alpha} \sim 10^{44} \text{ erg s}^{-1}$ (e.g., Steidel et al. 2000; Francis et al. 2001; Matsuda et al. 2004; Dey et al. 2005; Nilsson et al. 2006; Yang et al. 2009, 2010; Matsuda et al. 2011; Prescott et al. 2012). Recently, Hayes et al. (2011) discovered a polarization pattern of concentric rings within a $\text{Ly}\alpha$ nebula at $z = 3.1$, which supports a central powering mechanism within the nebula. While the physical scale of $\text{Ly}\alpha$ nebulae ($\sim 100 \text{ kpc}$) is much larger than that of AGN central engines ($\sim 1 \text{ pc}$), the basic pictures are the same: $\text{Ly}\alpha$ or continuum photons from the central source are resonantly or Rayleigh scattered by the surrounding neutral H I medium. However, theoretical modeling of the $\text{Ly}\alpha$ polarization is still in its infancy (Dijkstra & Loeb 2008), and therefore a detailed modeling of $\text{Ly}\alpha$ polarization in diverse geometry is required.

We compute, in this paper, the polarization of the far UV radiation around $\text{Ly}\alpha$ that is Rayleigh scattered in a thick neutral hydrogen region. The paper is composed as follows. In section 2, we discuss the atomic physics of Rayleigh scattering around $\text{Ly}\alpha$. In the following section, the scattering geometry and our Monte Carlo code are described. The main result is presented in section 3. In section 4 we discuss the observational implications of polarized $\text{Ly}\alpha$ in an AGN.

2 ATOMIC PHYSICS OF RAYLEIGH SCATTERING

There have been many basic research works on the Rayleigh scattering processes (e.g. Isliker et al. 1989, Gavrilu 1967, Sadeghpour & Dalgarno 1992, Lee 2013). The time-dependent second order perturbation theory is used to describe the Rayleigh scattering process. The scattering cross section is given by the Kramers-Heisenberg formula,

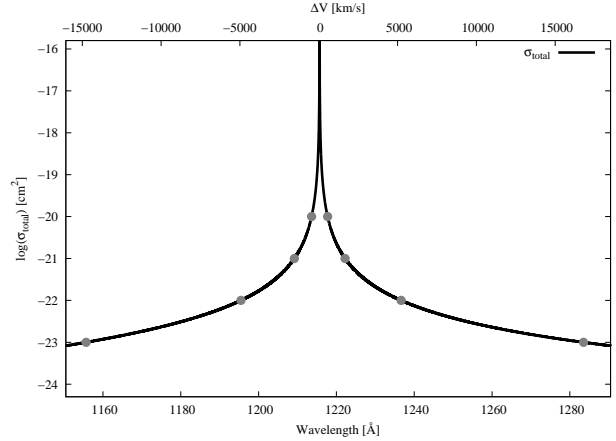


Figure 1. Cross section for Rayleigh scattering by atomic hydrogen. The vertical scale is logarithmic, whereas the horizontal axis is wavelength in units of Å. The dots mark the wavelengths having the cross section values of 10^{-20} , 10^{-21} , 10^{-22} , 10^{-23} cm^2 . The cross section exhibits redward asymmetry as pointed out by Lee (2013).

which can be written as

$$\frac{d\sigma_{Ray}}{d\Omega} = r_0^2 \left| (\epsilon^\alpha \cdot \epsilon^{\alpha'}) \left(\sum_n M^b(n) + \int_0^\infty dn' M^c(n') \right) \right|^2. \quad (1)$$

Here, ϵ^α and $\epsilon^{\alpha'}$ are the polarization vectors associated with the incident and outgoing photons, respectively, and r_0 is the classical electron radius. The angular integral over the two polarization states for an incident unpolarized radiation results in the factor of $8\pi/3$, which is in turn multiplied by r_0^2 to yield the Thomson scattering cross section $\sigma_T = 0.665 \times 10^{-24} \text{ cm}^2$. In the formula, the matrix elements between the ground $1s$ state and the bound np states are given by

$$M^b(n) = \frac{m\omega^2}{3\hbar} |\langle 1s || r || np \rangle|^2 \frac{2\omega_{n1}}{\omega_{n1}^2 - \omega^2}, \quad (2)$$

and those between $1s$ and continuum $n'p$ states are given by

$$M^c(n') = \frac{m\omega^2}{3\hbar} |\langle 1s || r || n'p \rangle|^2 \frac{2\omega_{n'1}}{\omega_{n'1}^2 - \omega^2}. \quad (3)$$

The explicit expressions of the reduced matrix elements can be found in many text books on quantum mechanics (e.g. Berestetskii et al. 1971, Saslow & Mills 1969). The Rayleigh scattering cross section is shown in Fig. 1, where the horizontal axis is wavelength in units of Å and the vertical scale is the logarithm of the cross section in units of cm^2 . A useful approximation to the Rayleigh scattering cross section can be also found in Lykins et al. (2015).

In particular, near $\text{Ly}\alpha$, the cross section is dominantly contributed by the first term in the summation leading to an approximation

$$\sigma_{Ray}(\lambda) \simeq \sigma_T \left[\frac{f_\alpha}{(\lambda/\lambda_\alpha) - 1} \right]^2, \quad (4)$$

where $f_\alpha = 0.4162$ is the oscillator strength for the $\text{Ly}\alpha$ transition and $\lambda_\alpha = 1215.67 \text{ Å}$ is the $\text{Ly}\alpha$ wavelength.

Given a neutral column density N_{HI} , we may consider the scattering band width $\Delta\lambda_R(N_{HI}) = \lambda - \lambda_\alpha$ by the wavelength width around $\text{Ly}\alpha$, for which the Rayleigh scattering

optical depth exceeds unity. Corresponding to $\Delta\lambda_R(N_{HI})$, we have the Doppler velocity width $\Delta V = c(\lambda - \lambda_\alpha)/\lambda_\alpha$. The requirement $\sigma_{Ray}(\lambda)N_{HI} = 1$ leads to

$$\left(\frac{\Delta V}{c}\right)^2 \simeq \sigma_T N_{HI} c^2 f_{12}^2, \quad (5)$$

or numerically

$$\frac{\Delta V}{10^4 \text{ km s}^{-1}} \simeq \left[\frac{N_{HI}}{3 \times 10^{22} \text{ cm}^{-2}} \right]^{1/2}. \quad (6)$$

Because the dynamical velocity scale of the broad line region of a typical AGN is about 10^4 km s^{-1} , most of the broad Ly α line photons can be Rayleigh scattered under the assumption that $N_{HI} \geq 3 \times 10^{22} \text{ cm}^{-2}$. This velocity scale is much larger than the thermal speed of typically photoionized emission nebulae, no consideration is made of resonance scattering of Ly α in this work (e.g. [Dijkstra & Loeb 2008](#)).

The dots in Fig. 1 correspond to those wavelengths with Rayleigh scattering optical thickness τ_s from 0.1 to 100 for H I column density of $N_{HI} = 10^{21} \text{ cm}^{-2}$. As is noted in these values, the asymmetry in the Rayleigh cross section is quite significant (see also [Totani et al. 2016](#) and [Bach & Lee 2014](#)). Therefore we expect that the effect of asymmetry in scattering cross section will be apparent in the flux profile and polarization of Rayleigh scattered radiation.

In this work, we consider far UV radiation in the fixed wavelength range $\lambda_\alpha - 70 \text{ \AA} < \lambda < \lambda_\alpha + 70 \text{ \AA}$, and the cross section at the lower and upper wavelength limits is $\sim 10^{-25} \text{ cm}^2$.

3 MONTE CARLO SIMULATIONS OF RAYLEIGH SCATTERING

3.1 Scattering Geometry

In this section, we illustrate the scattering geometry adopted in this work. We consider a neutral hydrogen region in the shape of a slab with a finite thickness and infinite lateral extension. The slab geometry is a convenient model to study the fundamental properties of the polarization of Rayleigh scattered radiation and verify the Monte Carlo code as well. In this case, the H I column density N_{HI} along the normal direction completely specifies the scattering geometry.

The other scattering geometry considered in this work is a finite cylindrical shell which is characterized by the height H and the inner and outer radii R_i and R_o , respectively. In this work, we set the parameters $R_o = 2R_i$ so that the inner radius is the same as the lateral width of the shell. There are two controlling parameters for this geometry. One is the H I column density $N_{HI} = n_{HI}(R_o - R_i)$ in the lateral direction and the other is the shape parameter given by the ratio $A = H/R_i$.

A schematic illustration of our scattering geometry is shown in Fig. 2. We set the coordinate system so that z -axis coincides with the symmetry axis and that the Ly α emission source is located at the origin. In our Monte Carlo simulations we collect emergent photons according to the z component $\mu_o = \cos\theta_o$ of the unit wavevector $\hat{\mathbf{k}}$ with the bin size of $\Delta\mu_o = 0.1$. In the slab case, the Ly α emission source is located on the negative z -axis, so that we will refer emergent photons with negative and positive μ_o to Rayleigh reflected and transmitted photons, respectively.

In this work, we consider two types of incident radiation, one consisting of pure flat continuum and the other with an additional contribution of broad Ly α emission with a triangular profile. The triangular profile is chosen for simplicity of interpretation. The equivalent width of the Ly α emission is set to be 90 \AA and the FWHM (full width at half maximum) of that is 20 \AA , $\simeq 5000 \text{ km/s}$ in the scale of speed, which appears to be typical in many AGNs ([Vanden Berk et al. 2001](#)).

The density matrix formalism is adopted in our Monte Carlo code to describe the polarization information. A 2×2 density matrix ρ is defined by

$$\rho = \begin{pmatrix} (I+Q)/2 & (U+iV)/2 \\ (U-iV)/2 & (I-Q)/2 \end{pmatrix} \quad (7)$$

in terms of the Stokes parameters I, Q, U and V (see e.g. [Ahn & Lee 2015](#)).

In this simulation the two polarization basis vectors associated with the unit wavevector $\hat{\mathbf{k}} = (\sin\theta \cos\phi, \sin\theta \sin\phi, \cos\theta)$ are chosen as

$$\begin{aligned} \epsilon_1 &= (-\sin\phi, \cos\phi, 0) \\ \epsilon_2 &= (\cos\theta \cos\phi, \cos\theta \sin\phi, -\sin\theta) \end{aligned} \quad (8)$$

so that the ϵ_1 and ϵ_2 represent the polarization in the direction perpendicular and parallel to the symmetry axis, respectively.

For each photon generated in the simulation, a density matrix with a unit trace is assigned and followed until escape. Being characterized by the density matrix elements $\rho_{11} = \rho_{22} = 0.5$, $\rho_{12} = \rho_{21} = 0$, the initial photon from the source is assumed to be completely unpolarized.

According to [Schmid \(1995\)](#) the polarization of Rayleigh scattered radiation is characterized by the same phase function as that of Thomson scattering. The unnormalized density matrix ρ'_p associated with the scattered photon with a new unit wavevector $\hat{\mathbf{k}}' = (\sin\theta' \cos\phi', \sin\theta' \sin\phi', \cos\theta')$ is computed using the equation

$$(\rho'_p)_{ij} = \sum_{kl=1,2} (\epsilon'_i \cdot \epsilon_k) \rho_{kl} (\epsilon_l \cdot \epsilon'_j). \quad (9)$$

The components are explicitly written as

$$\begin{aligned} (\rho'_p)_{11} &= (\cos^2 \Delta\phi) \rho_{11} \\ &\quad - (\cos\theta \sin 2\Delta\phi) \rho_{12} \\ &\quad + (\sin^2 \Delta\phi \cos^2 \theta) \rho_{22} \\ (\rho'_p)_{12} &= \left(\frac{1}{2} \cos\theta' \sin 2\Delta\phi\right) \rho_{11} \\ &\quad + (\cos\theta \cos\theta' \cos 2\Delta\phi + \sin\theta \sin\theta' \cos \Delta\phi) \rho_{12} \\ &\quad - \cos\theta (\sin\theta \sin\theta' \sin \Delta\phi + \frac{1}{2} \cos\theta \cos\theta' \sin 2\Delta\phi) \rho_{22} \\ (\rho'_p)_{22} &= (\cos^2 \theta' \sin^2 \Delta\phi) \rho_{11} \\ &\quad + \cos\theta' (2 \sin\theta \sin\theta' \sin \Delta\phi + \cos\theta \cos\theta' \sin 2\Delta\phi) \rho_{12} \\ &\quad + (\cos\theta \cos\theta' \cos \Delta\phi + \sin\theta \sin\theta')^2 \rho_{22} \end{aligned} \quad (10)$$

The trace of the unnormalized density matrix represents the angular distribution of the scattered radiation, from which we select θ' and ϕ' in a probabilistic way ([Lee et al. 1994](#)). Once the selection is made, the density matrix is normalized to have a unit trace. In the density matrix formalism adopted in this work, the off diagonal element ρ_{12} remains real because Rayleigh scattering induces no circular

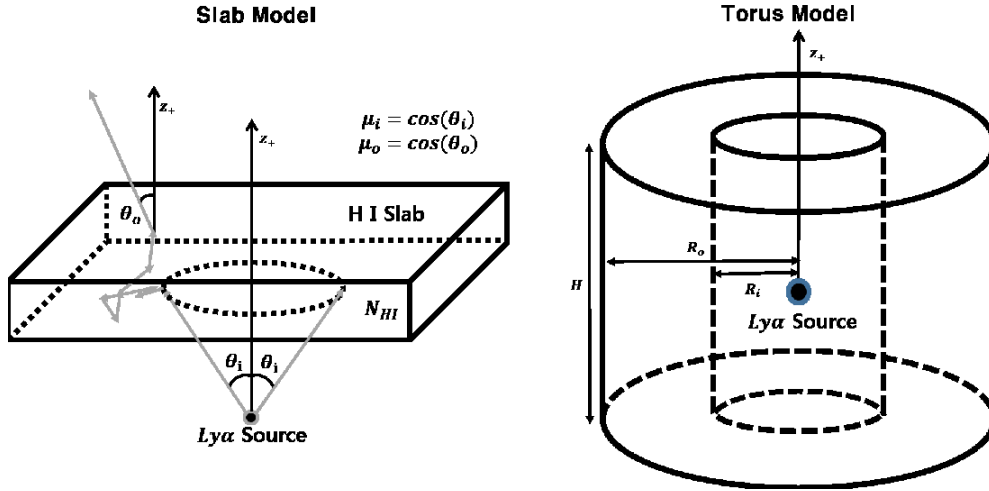


Figure 2. Schematic illustration of the scattering geometry adopted in this work. The Ly α emission source is located at the center of the coordinate system. In the case of the slab geometry, hydrogen atoms are uniformly distributed between $z = z_0 > 0$ and $z = z_0 + H$, where H is the thickness of the slab. The column density N_{HI} is measured along the z -direction in the slab geometry. In the torus geometry, hydrogen atoms are uniformly distributed inside a cylinder shell characterized by the inner and outer radii R_i and $R_o = 2R_i$ and the height $H = AR_i$.

polarization for an incident radiation with no circular polarization. In other words, the density matrix in this work is a 2×2 real symmetric matrix. Furthermore, due to the axial symmetry of the scattering geometry considered in this work, linear polarization can develop only in the direction parallel or perpendicular to the symmetry axis when spatially averaged, leading to the vanishing average of ρ_{12} . The resultant linear polarization Q is represented by the difference of the two diagonal elements of ρ with a unit trace,

$$Q = \rho_{11} - \rho_{22}. \quad (11)$$

Here, a positive Q implies that the polarization develops in the direction perpendicular to the symmetry axis, whereas a negative Q shows polarization in the parallel direction. The scattering geometries considered in this work possess axis-symmetry and our choice of the Stokes parameter Q to represent polarization along the symmetry axis makes the Stokes parameter U vanish.

3.2 Rayleigh Scattering in a Slab Region

In this section, we present our Monte Carlo results for Rayleigh scattering in a slab. Note that in sections 3.2.1 and 3.2.2, we only collect photons that are scattered at least once and neglect optically thin photons that pass through the slab without any interaction because our goal is to investigate the polarization properties of the Rayleigh scattered photons depending on the μ_o , μ_i , and N_{HI} .

In section 3.2.3, we integrate over all μ_i to investigate the flux and polarization of radiation originated from an isotropic source. We also generate mock spectra using a flat continuum source and a emission source with a triangular profile.

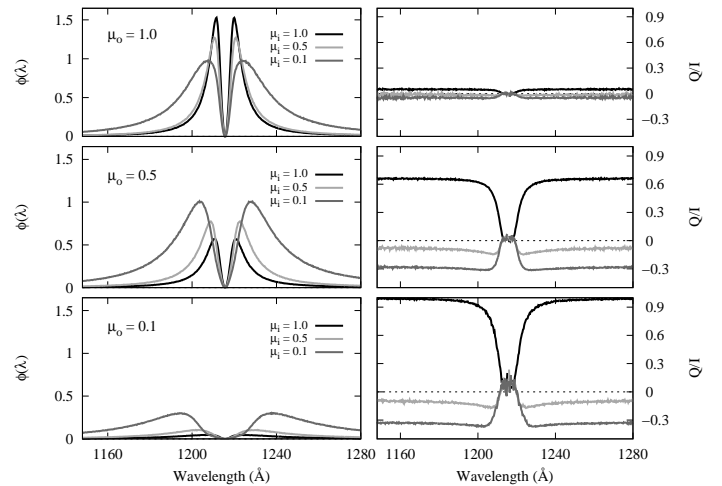


Figure 3. Degree of linear polarization (right panels) and flux (left panels) of far UV flat continuum around Ly α that are Rayleigh transmitted from a slab with the H I column density $N_{HI} = 10^{21} \text{ cm}^{-2}$ in the normal direction. The upper, middle and bottom panels are for those photons emergent with μ_o in the interval (0.9, 1), (0.4, 0.5) and (0, 0.1), respectively. In the right panels, a positive Q/I implies polarization in the direction perpendicular to the slab normal.

3.2.1 Spectra of Reflected and Transmitted Radiation

In Fig. 3, we show the flux (left panels) and polarization degree (right panels) for Rayleigh transmitted radiation from a slab with the H I column density of $N_{HI} = 10^{22} \text{ cm}^{-2}$ in the normal direction. The far UV incident radiation is to be taken as a flat continuum, characterized by the same number of photons emitted with specified μ_i per unit wavelength interval. Here μ_i represent the z -component of the unit vector in the direction of the incident photons. The upper pan-

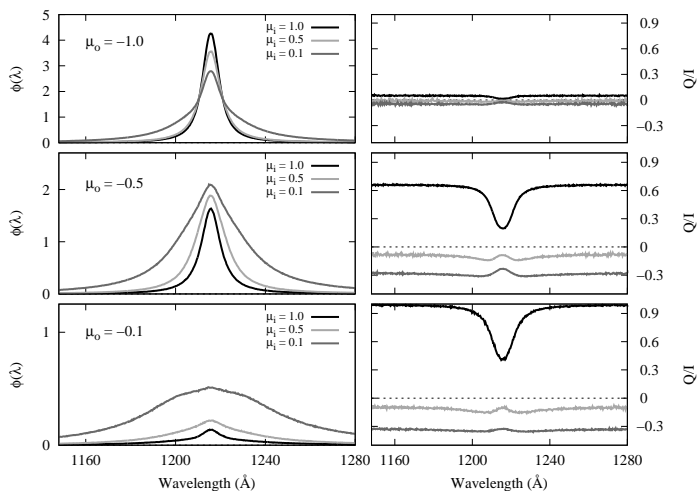


Figure 4. Polarization and flux of far UV flat continuum around Ly α Rayleigh reflected from the same slab considered in Fig. 3. The upper, middle and bottom panels are for those photons emergent with μ_o in the interval $(-1, -0.9)$, $(-0.5, -0.4)$ and $(-0.1, 0)$, respectively.

els are flux and degree of polarization of photons emergent with μ_o between 0.9 and 1.0. The middle and bottom panels show the same information for μ_o in the intervals $(0.4, 0.5)$ and $(0, 0.1)$, respectively.

The left panels show the flux profiles for various μ_i and μ_o . All the transmitted profiles are characterized by the central dip of which the width increases as μ_o decreases from 1 to 0. This implies that the central dip reflects the H I column density of the slab in the direction of incidence. On the other hand, the much extended wing features delineate the scattering cross section that is approximated by a Lorentzian. Being optically thin, most far UV radiation in this wavelength regime will pass through the slab without any interaction with atomic hydrogen.

When $\mu_o \sim 1$, the degree of polarization is nearly zero due to the axial symmetry. This is illustrated in the right top panel, where irrespective of μ_i , Q/I is negligibly small. This case may serve as a check of our code.

An opposite case can be seen in the right bottom panel. For $\mu_i \sim 1$ and $\mu_o \sim 0.1$ corresponding to the normal incidence and emergence in the grazing direction, the degree of polarization in the wing region is nearly 1 in the direction perpendicular to the slab normal (z axis in Fig. 2). However, near line center the polarization becomes quite weak due to the sharp increase of scattering optical depth.

It is interesting to observe that $\mu_i \simeq 0.1$ and $\mu_o \sim 0.1$ the polarization develops in the direction parallel to the symmetry axis with a typical degree of polarization about 30 % in the wing part. This is because most photons are singly scattered at the large distance from the origin, thus strongly polarized in a direction parallel to the symmetry axis given that the wavevectors of the incident and transmitted photons are located within $z \sim 0$ plane.

In this case also the polarization becomes rapidly weak as the scattering optical depth increases toward the line center. For $\mu_i \simeq 0.5$ and $\mu_o \simeq 0.1$, the polarization is very weak because it corresponds to an intermediate case of the two

cases of the normal and grazing incidences. The middle panels show the intermediate behavior between that of the case $\mu_o = 1$ shown in the top panels and that for $\mu_o = 0.1$.

In Fig. 4, we show our results for Rayleigh reflected radiation near Ly α from the same slab considered in Fig. 3. In the left panels showing the flux as a function of wavelength, we immediately note that all the profiles are characterized by a single broad peak of which the width is dependent on the incident and emergent directions. The photons constituting the central peak are optically so thick that they rarely penetrate to contribute to the transmitted flux considered in Fig. 3.

In the right panels, we show the degree of linear polarization of the Rayleigh reflected radiation. In the top panel, the radiation is negligibly polarized because the observer's line of sight nearly coincide with the symmetry axis. An interesting point can be noted in the middle and bottom panels for $\mu_i = 1$. In these cases the center part is the most weakly polarized but still exhibits fairly high degree of linear polarization in excess in 10 per cent. This is highly contrasted with the negligibly polarized cases of the transmitted flux shown in the middle and bottom panels of Fig. 3.

This contrasting behavior can be understood by considering the fact that the reflected flux is quite significantly contributed by the singly Rayleigh scattered near the point of entry. These singly scattered photons are highly polarized in the direction perpendicular to the symmetry axis. However, near the Ly α center in the transmitted flux we expect no such singly scattered photons due to the huge scattering optical depths. This leads to negligibly polarized dip in the transmitted flux.

Another interesting point to be noted is the fact that we have a fairly constant degree of linear polarization for the cases of oblique and grazing incidence where $\mu_i \leq 0.5$. This phenomenon is also attributed to the fact that most contribution is made by photons scattered only a few times irrespective of wavelength.

3.2.2 Effects of H I Column Density

In Fig. 5, we show the polarization behavior as a function of emergent direction for two values of $N_{HI} = 10^{21} \text{ cm}^{-2}$ (top panels) and 10^{23} cm^{-2} (bottom panels). The horizontal axis shows μ_o , where $\mu_o < 0$ is for Rayleigh reflected radiation and $\mu_o > 0$ for Rayleigh transmitted radiation. The different symbols represent various values of μ_i .

We also divide the incident radiation into two parts depending on the scattering optical thickness so that the left panels show the emergent photons for $\tau_s < 10$ (wing) and the right panels for $\tau_s > 10$ (core). The wavelengths corresponding to $\tau_s = 10$ for $N_{HI} = 10^{21} \text{ cm}^{-2}$ are $\lambda_1 = 1213.61 \text{ \AA}$ and $\lambda_2 = 1217.74 \text{ \AA}$. For $N_{HI} = 10^{23} \text{ cm}^{-2}$ the corresponding wavelengths are $\lambda_3 = 1195.45 \text{ \AA}$ and $\lambda_4 = 1236.62 \text{ \AA}$.

Because the incident radiation is prepared in the wavelength range $\lambda_\alpha - 70 \text{ \AA} < \lambda < \lambda_\alpha + 70 \text{ \AA}$ throughout all the Monte Carlo simulations presented in this work, the larger wavelength range for $\tau_s < 10$ for $N_{HI} = 10^{21} \text{ cm}^{-2}$ than for $N_{HI} = 10^{23} \text{ cm}^{-2}$ implies that the slab in the case of top left panel is optically thin to more incident photons than in the case of bottom left. The Rayleigh scattering phase function is forward and backward symmetric so that an optically thin slab shows the same polarization behavior for transmitted

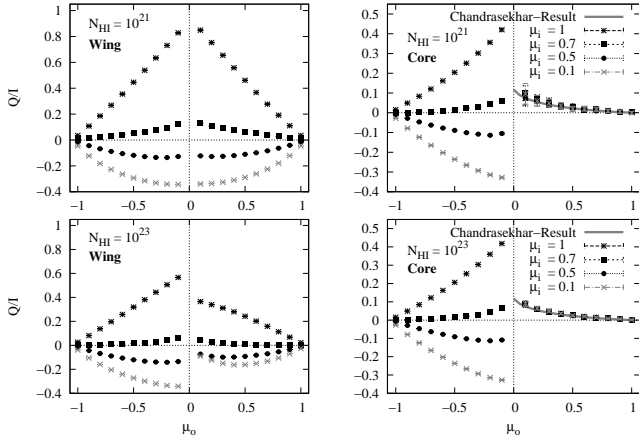


Figure 5. Polarization behaviors for wing photons $\tau_s < 10$ Rayleigh scattered from a slab (left panels) and for core photons $\tau_s > 10$ (right panels). In order to find the dependence on H I density, we consider two cases of $N_{HI} = 10^{21} \text{ cm}^{-2}$ (top panels) and $N_{HI} = 10^{23} \text{ cm}^{-2}$. The horizontal axis shows μ_o , where $\mu_o < 0$ is for Rayleigh reflected radiation and $\mu_o > 0$ for Rayleigh transmitted radiation.

and reflected components. This is illustrated in the symmetric polarization with respect to $\mu_o = 0$ in the top left panel. In the bottom left panel for $N_{HI} = 10^{23} \text{ cm}^{-2}$ symmetry is significantly broken due to more contribution from photons with optical depths exceeding unity. These photons with optical depths greater than unity will be scattered many times to become quite weakly polarized. This tendency becomes more severe for photons emergent near the grazing direction ($\mu_o = 0$). Therefore, optically thin Rayleigh reflected radiation is maximally polarized in the grazing direction, whereas it is no longer the case for Rayleigh transmitted radiation from grazing incidence ($\mu_i = 0$).

This observation is confirmed in the behaviors shown in the right panels, where all the photons are characterized by $\tau_s > 10$. Rayleigh reflected components are significantly contributed by photons with a small number of scatterings leading to strong polarization. Maximal asymmetry is obtained for photons emergent in the grazing direction, which leads to maximum degree of polarization. This also explains again the stronger polarization shown in the spectra of Rayleigh reflected radiation than in those of Rayleigh transmitted radiation illustrated in Figs. 3 and 4.

A very interesting behavior of Rayleigh transmitted radiation is recognized in the right panels, where the scattering optical depths are very large. The polarization develops in the direction perpendicular to the slab normal independent of μ_i . Furthermore, the degree of polarization increases as μ_o approaches 0 from 1. The limit value is 11.7 %, which was obtained by Chandrasekhar (1960) in the polarized transfer of Thomson scattered radiation in an infinitely thick slab (see also Angel 1969). A similar result was obtained by Ahn & Lee (2015) in their study of the polarized transfer of resonantly scattered Ly α .

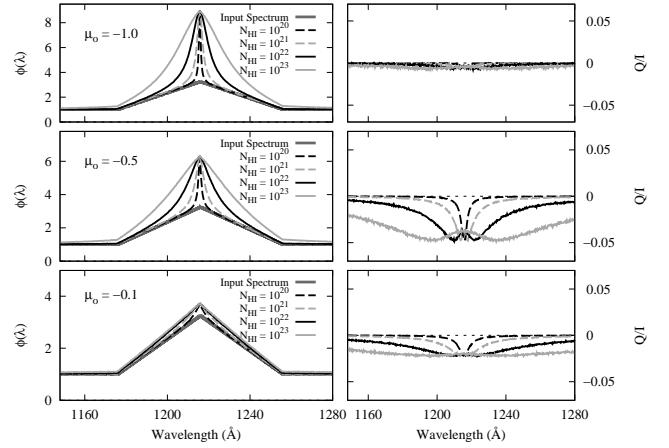


Figure 6. Rayleigh reflected degree of polarization(right panel) and flux(left panel) of the isotropic source composed the flat continuum and broad emission. The various lines are shown by H I column densities N_{HI} of slab model.

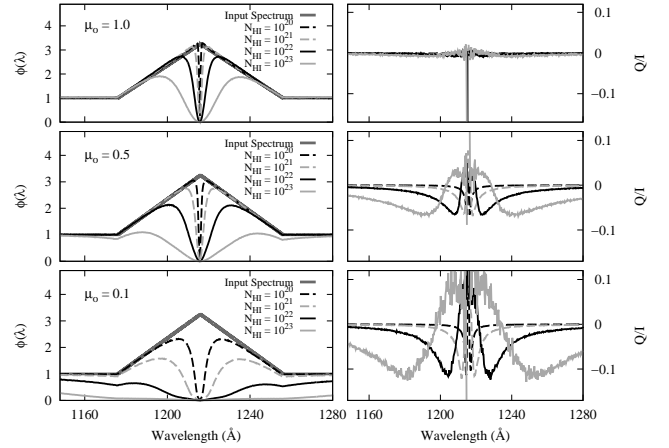


Figure 7. Transmitted component of same model as Fig. 6.

3.2.3 Polarized Ly α from an Isotropic Source

In previous sections, we considered photons only scattered at least once by hydrogen atoms, in which case non-scattered radiation would reduce the observed polarization significantly. In contrast in this section we consider an isotropic source and collect all the photons including those without being Rayleigh scattered. In Figs. 6 and 7, we show the polarization of Rayleigh scattered radiation in a slab illuminated by an isotropic source for 4 different values of N_{HI} . The input spectrum is the sum of a flat continuum and a broad Ly α emission line flux with a triangular profile described in section 3.1. The top panel of Fig. 6 shows the Rayleigh reflected component emergent in the normal direction, which is negligibly polarized due to symmetry.

Because the covering factor of the scattering region with respect to the emission source is 50 %, the emergent flux is significantly distorted in the wavelength region with $\tau_s > 10$ leading to the formation of the sharp central feature for

low values of N_{HI} . As shown in the bottom left panel, the Rayleigh reflected in the grazing direction shows almost the same profile as the incident radiation. This is due to large τ_s in this direction, giving rise to full reflection of the incident radiation.

Rayleigh reflected radiation in a slab is polarized in the direction parallel to the symmetry axis, which is illustrated by the negative degree of linear polarization in the right panels of Fig. 6. Strong polarization is obtained in the case of $\mu_o = -0.5$ and weak polarization is seen for the Rayleigh reflected radiation emergent in the grazing direction. In the far wing region where the scattering optical thickness is very small, we obtain very weak polarization. It is notable that there exist local maxima in the degree of linear polarization (minima in Q/I value) around the shoulder region for $\mu_o = -0.5$. Here, the term 'shoulder region' is meant to indicate the intermediate region between the core and wing parts. This is explained by the fact that the line center is contributed more significantly by photons scattered many times and hence polarized very weakly than the shoulder region is.

The left panels of Fig. 7 show the spectra of Rayleigh transmitted radiation from an isotropic source with a triangular broad Ly α emission. As is previously pointed out, the spectra are characterized by the central dip that depends on the emergent direction and N_{HI} . In the middle right panel and the bottom right panel, the degree of polarization exhibits a complicated behavior. The degree of polarization is positive near line center and negative from the shoulder and wing regions.

This complicated behavior can be understood as follows. For a very optically thick photon the radiative transfer through a thick slab must involve a diffusive propagation along the vertical z -direction until it reaches a slab boundary before escape. The diffusive propagation along z -direction induces development of polarization in the direction perpendicular to z -axis. For photons emergent in the grazing direction, the degree of polarization can reach 11.7 per cent, which was shown by Chandrasekhar (1960) and illustrated in the bottom right panel of Fig. 7. However, in the far wing regions where photons are optically thin, scattering plane nearly coincides with the slab plane leading to polarization in the direction parallel to z -axis. An analogous phenomenon can be found in the case of Thomson scattering investigated by Phillips & Meszaros (1986). We point out that the polarization flip around Ly α can be an important signature of Rayleigh transmitted Ly α in a thick neutral slab and that the wavelength at which the flip occurs indicates the characteristic neutral column density of the slab.

The left and right panels of Fig. 8 show the polarization behaviors of radiation with low and high Rayleigh scattering optical depths, respectively. In this figure, the simulation parameters are the same as in Figs. 6 and 7.

In the left panel, the wing photons both Rayleigh reflected and transmitted are polarized in the direction parallel to the symmetry axis. For small values of $N_{HI} \leq 10^{21} \text{ cm}^{-2}$ the polarization behaviors are similar for Rayleigh reflected and transmitted components. However, for a very thick $N_{HI} = 10^{23} \text{ cm}^{-2}$ the degree of polarization peaks at $\mu_o \simeq 0$ for Rayleigh transmitted radiation, because they are significantly contributed by singly scattered photons.

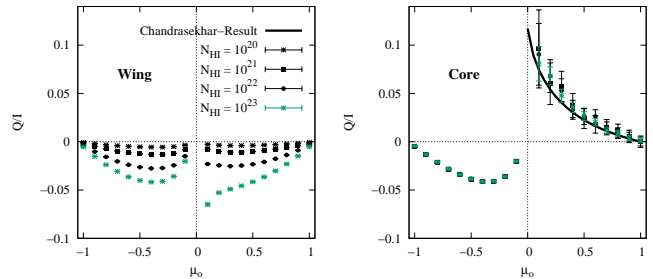


Figure 8. Degree of polarization for wing photons(left panel) and core photons(right panel). $\mu_o < 0$ is for reflected component and $\mu_o > 0$ is for transmitted component.

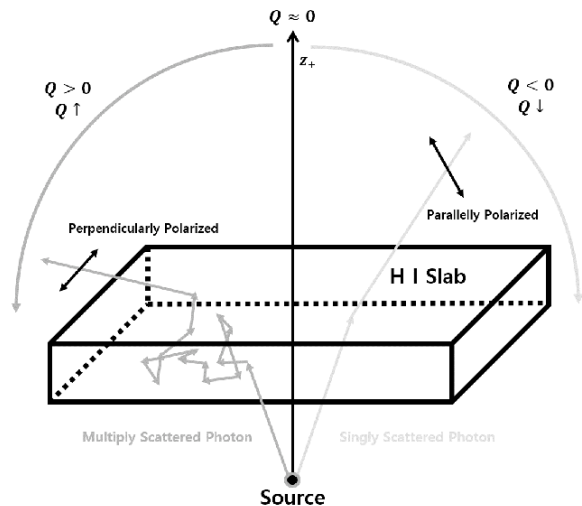


Figure 9. Description of degree of polarization for optically thin and thick cases in the slab model.

In the right panel we notice that the Rayleigh reflected radiation is always polarized in the direction parallel to the symmetry axis irrespective of the Rayleigh scattering optical depth. However, Rayleigh transmitted radiation can be polarized in the direction perpendicular to the symmetry axis only when the Rayleigh scattering optical depth is very high.

In Fig. 9, we schematically illustrate polarization behaviors of Rayleigh scattered photons in optically thin and thick cases. Multiply scattered photons tend to be polarized in the direction perpendicular to the symmetry axis as a result of diffusive propagation along z -axis, whereas singly scattered photons are polarized in the direction parallel to z -axis.

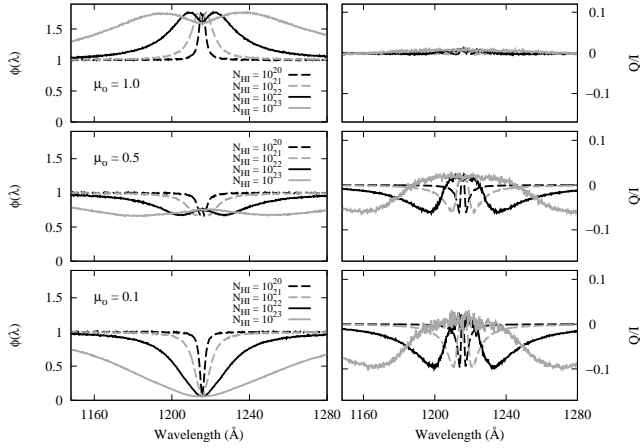


Figure 10. Flux and degree of polarization of flat continuum incident on and Rayleigh scattered in a torus with the shape parameter $A = 2$.

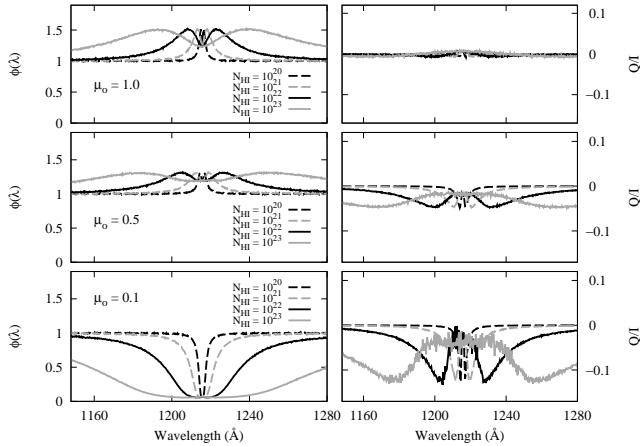


Figure 11. Same data as in Fig. 10 except for $A = 1$. No polarization flip occurs in this case.

3.3 Rayleigh Scattering in a Torus Region

In this section, we consider Rayleigh scattered radiation in a cylindrical shell region, which approximates the torus geometry that is invoked in the unification model of AGNs. The torus geometry is symmetric with respect to the plane $z = 0$, and hence the discussion is limited to radiation emergent with $\mu_o > 0$. In this work, the shape of the cylindrical shell is described by the parameter $A = H/R_i$ defined as the ratio of the height and the inner radius.

3.3.1 Spectra and Polarization of Flat Continuum

In Fig. 10 we show the flux and polarization of Rayleigh scattered radiation emergent from a torus with $A = 1$ for 4 different values of the H I column density. The incident radiation is pure flat continuum. The top panels show the spectra and degree of polarization emerging along the symmetry axis (analogous to type 1 AGNs). Because of symme-

try the emergent radiation is nearly unpolarized. The flux profile exhibits local blue and red maxima. In particular, for $N_{HI} = 10^{23} \text{ cm}^{-2}$ the maxima are seen at $\lambda = 1187 \text{ \AA}$ and $\lambda = 1242 \text{ \AA}$. At these wavelengths the scattering optical depth is near unity and the whole scattering region contributes to the flux emergent in the direction near z -axis.

The middle panels show the simulated data collected for photons emerging with $\mu_o = 0.5$. As is seen in the left panel, the central part is absorbed because the observer's line of sight is blocked by the cylindrical shell. At the line center we notice a small mound of Rayleigh scattered flux so that the flux minima are found at positions shifted redward and blueward of the line center. The formation of the central mound is attributed to a large number of bouncing near the inner surface of the cylindrical shell by those photons with huge scattering optical depth τ_s . Through repeated bouncings they climb up the inner cylindrical shell until they reach the upper part where direct escape to the line of sight with $\mu_o = 0.5$ is readily made. Therefore, these photons are polarized in the direction perpendicular to the symmetry axis. This explains the positive degree of polarization shown by those photons in the vicinity of the central mound illustrated in the right panel. In the far wing regions where photons are optically thin, the polarization develops in the direction parallel to the symmetry axis.

The bottom panel shows the spectra and polarization for grazingly emergent radiation (analogous to type 2 AGNs). In this case we observe a simple central dip in the left panel because of the negligible area in the upper part of the cylindrical shell where direct escape is possible. Polarization near the line center is very weak and hence significant polarization along the symmetry axis can be observed in the wing regions.

In Fig. 11, we plot the same Monte Carlo result for a torus with $A = 1$. In the middle panel of this figure, we notice that the polarization develops in the direction parallel to the symmetry axis in the entire range of wavelength, and no polarization flip is seen. This is in high contrast with the behavior shown in the middle panel of Fig. 10. The torus geometry with a low value of $A = 1$ allows mainly Rayleigh scattering in the plane nearly perpendicular to the symmetry axis, resulting in polarization developing in the direction parallel to the symmetry axis. The presence of polarization flip in Rayleigh scattered Ly α may indicate quite significant covering factor of the molecular torus in AGNs.

In the bottom panel we notice the polarization behavior of the grazingly emergent radiation qualitatively similar to that found in the middle panel. For photons with Rayleigh scattering optical depth τ_s near unity, single Rayleigh scattering dominates in the plane nearly coinciding with the $x - y$ plane, which leads to strong polarization in the parallel direction with the degree of polarization in excess of 10 percent. The weak polarization near the line center shows the effect of multiple scatterings that tend to randomize the electric field associated with the scattered radiation.

In Fig. 12, we illustrate the development of polarization in a torus model. In the tall and optically thick torus, photons tend to be polarized in the direction perpendicular to the vertical axis as they diffuse along the vertical direction through a large number of scattering near the inner wall. This behavior is similar to one considered in the optically thick case shown in Fig. 9 and explains the polarization flip

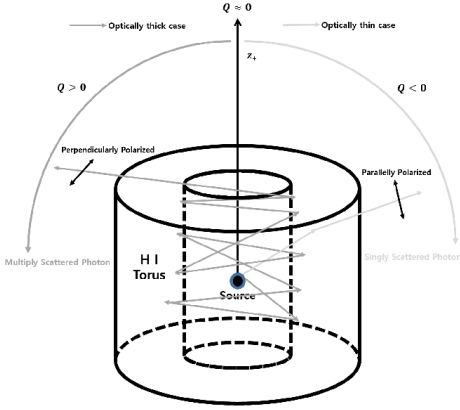


Figure 12. Illustration of polarization development in a scattering region with a torus shape. In the case of an optically thick and tall torus, diffusion along the vertical direction tends to orient the electric field in the direction perpendicular to the symmetry axis. In the case of an optically thin torus, emergent light is polarized parallelly to the symmetry axis.

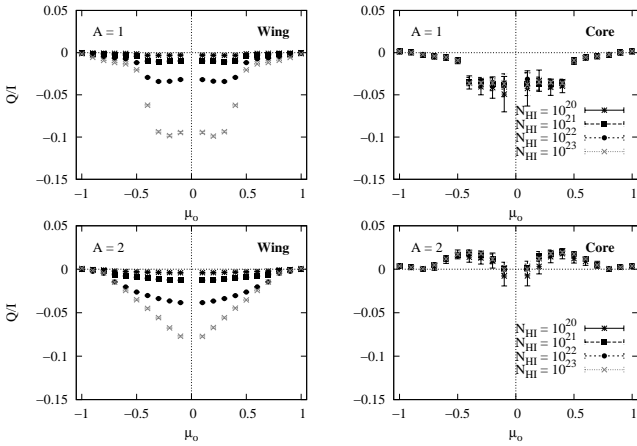


Figure 13. Angular distribution of the polarization of Rayleigh scattered from a torus. The left panels are for wing photons $\tau_s < 10$ and the right panels are for core photons ($\tau_s > 10$).

in Fig. 10. In the case of an optically thin torus, emergent radiation is polarized in the direction parallel to the symmetry axis. This is also similar to the polarization behavior found in the optically thin slab model.

3.3.2 Effects of H I Column Density and Covering Factor

In Fig. 13 we show the angular distributions of the polarization of Rayleigh scattered from tori with the two values of $A = 1$ and $A = 2$. Four different values of N_{HI} are investigated. In the figure, we divide the incident radiation by the scattering optical depth τ_s in order to clarify the different behaviors of wing photons and core ones.

In the left panels we show the polarization of wing photons ($\tau_s < 10$), all of which are polarized in the direction parallel to the symmetry axis. In the top left panel for the case of $A = 1$, we notice that maximum degree of polarization is not seen for grazingly emergent radiation but $\mu_o \simeq 0.2$. This

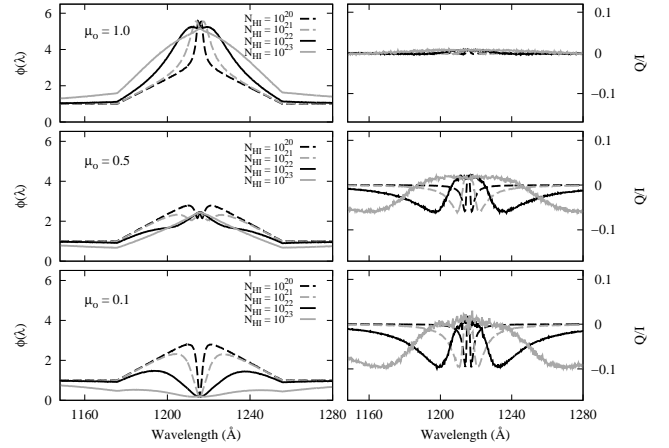


Figure 14. Degree of polarization and flux of broad emission and flat continuum incidence source. In this torus model, the shape parameter A is 2.

is in contrast with the case of $A = 2$ shown in the bottom left panel. In the case of $A = 1$, the polarization behavior resembles that of the wing photons reflected in a slab illustrated in Fig. 8. However, in the case of $A = 2$ the polarization behavior resembles that of the transmitted component.

Totally different behaviors are noticed in the case of the transfer of core photons ($\tau_s > 10$). In the top right panel for $A = 1$ all the core photons are polarized in the direction parallel to the symmetry axis, which is the same as their wing counterparts. The degree of polarization is smaller due to the increased number of scatterings required before escape for core photons. However, in the case of $A = 2$ shown in the bottom right panel, core photons are polarized in the perpendicular direction. In this scattering geometry, an core photon needs to climb up along the inner wall of the cylindrical shell by repeated bouncings before it makes the final exit of the scattering region. In the random walk type process of moving up and down along the inner wall, the electric field associated with the photon relaxes in the direction perpendicular to the symmetry axis. This situation is analogous to the perpendicular polarization that develops in the very optically thick slab investigated by Chandrasekhar (1960).

3.4 Mock Spectrum of AGNs in a Torus

In Fig. 14, we show our Monte Carlo simulated profiles and polarization of emergent radiation that is Rayleigh scattered in a torus region. The incident radiation consists of a flat continuum and a broad Ly α emission component with a triangular profile, which was considered in section 3.2.3.

The top panels show the data for radiation emergent nearly along the symmetry axis, which is negligibly polarized. However, the profiles are augmented by the Rayleigh scattered flux. For small $N_{HI} = 10^{20} \text{ cm}^{-2}$ Rayleigh scattering is limited to photons near line center leading to a spiky central feature.

In the middle panels for emergent radiation with $\mu_o \sim 0.5$, the behavior of polarization flip is apparent. The center part where the scattering optical thickness exceeds unity is polarized in the perpendicular direction. The wing regions

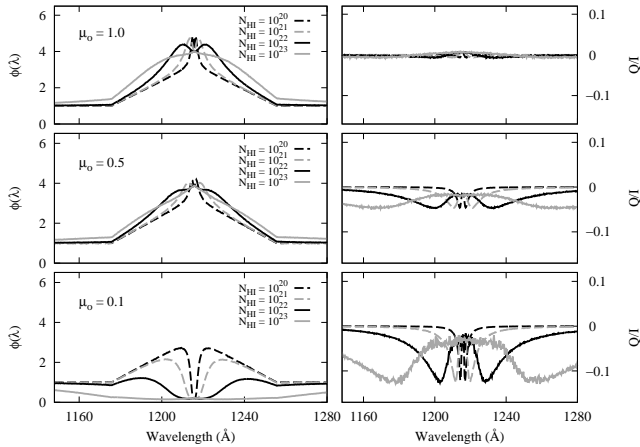


Figure 15. This figure is composed by same scheme as in Fig. 14 and $A = 1$.

exhibit polarization in the parallel direction due to dominant contribution from a small number of scattering occurring in the $x - y$ plane.

The bottom panel shows the simulated data for grazingly emergent radiation. The largest degree of polarization is obtained near the shoulder region with moderate scattering optical depth. In the far wing region where the scattering optical depth is very small, the degree of polarization is small due to the contribution from the unpolarized incident radiation that is not Rayleigh scattered.

Fig. 15 shows our Monte Carlo result for a short torus, for which the behavior is in high contrast with that illustrated in Fig. 14. In particular, in the middle panel, one can see that Rayleigh scattered radiation near $\text{Ly}\alpha$ is polarized in the direction parallel to the symmetry axis and no polarization flip appears. In the bottom panel for which the anisotropy is maximal, the degree of polarization is enhanced and particularly the shoulder part exhibits the degree of polarization in excess of 10 percent.

4 DISCUSSION AND SUMMARY

In this work, we compute the flux and polarization of the far UV radiation around $\text{Ly}\alpha$ Rayleigh scattered in a slab and a torus in order to develop a new spectropolarimetric tool to investigate the unification models of AGNs. In the slab geometry, the transmitted radiation is weakly polarized with the profile exhibiting a central dip in the flux whereas the Rayleigh reflected radiation is significantly polarized with an enhanced line center.

In the torus geometry we find an interesting behavior of polarization flip dependent on the shape of the torus. When the torus is tall with the shape parameter $A = H/R_i = 2$, the Rayleigh thick part near the line center is polarized in the direction perpendicular to the symmetry axis whereas the wing parts are polarized in the parallel direction. However in the case of a short torus model with $A = 1$, no polarization flip is observed and the emergent radiation is polarized in the direction parallel to the symmetry axis.

It has been proposed that hard X-ray background ra-

diation is significantly contributed by type 2 AGNs (e.g., Comastri et al. 1995). However, the population of type 2 AGNs is only poorly constrained (Gilli et al. 2007). According to AGN unification models, type 2 AGN population is closely related with the geometrical covering factor of the molecular torus. In view of this, detection of polarized $\text{Ly}\alpha$ exhibiting a polarization flip in the wing parts may indicate the presence of a tall molecular torus implying a fairly large population of type 2 AGNs.

The models adopted in this work are highly ideal and the H I distribution is more probably far from being axisymmetric. In this case, spectropolarimetric observations may reveal $\text{Ly}\alpha$ polarized in different directions depending on wavelength because the Rayleigh scattering optical thickness has no axisymmetry. In this work we made no consideration of narrow $\text{Ly}\alpha$ emission component, which may fill the central dip shown in the Rayleigh transmitted component and introduce an additional polarized component.

The Rayleigh scattering cross section is given as a squared sum consisting of contributions from each bound np and free $n'p$ state. For a photon in the vicinity of $\text{Ly}\alpha$, the $2p$ state provides a dominant contribution. A minor contribution from the remaining p states affects the final cross section in a complicated way so that the cross section is larger for radiation redward of $\text{Ly}\alpha$ than blueward (Lee 2013).

More quantitatively, for red and blue wavelengths around $\text{Ly}\alpha$, $\lambda_{\pm} = (1 \pm \Delta V/c)\lambda_{\alpha}$ corresponding to the Doppler velocity $\Delta V = 5,000 \text{ km s}^{-1}$, the asymmetry amounts to

$$\frac{\sigma(\lambda_+) - 1}{\sigma(\lambda_-)} \simeq 0.07. \quad (12)$$

The asymmetry amounting to 7 percent in scattering cross section will be more easily detected in the polarized flux than in the total flux. A small excess in the polarized flux redward of $\text{Ly}\alpha$ can be regarded as a convincing signature of Rayleigh scattering.

Lying at $+5,900 \text{ km s}^{-1}$ redward of $\text{Ly}\alpha$, the broad $\text{Nv}\lambda 1240$ line is often severely blended with the broad $\text{Ly}\alpha$ in many AGNs. This leads to the possibility that the Nv line photons can be Rayleigh scattered, which will also enhance the red part of $\text{Ly}\alpha$. However, the red enhancement due to Nv is expected to peak at $\Delta V = +5,900 \text{ km s}^{-1}$, whereas the red enhancement due to asymmetry in cross section is featureless.

One notable example is provided by Koratkar et al. (1995), who used the *Hubble Space Telescope* to perform spectropolarimetry of the quasar PG 1630+377. They reported that $\text{Ly}\alpha$ in this object is significantly polarized with the degree of polarization 7 per cent after correction for unpolarized continuum, whereas no evidence of strong polarization was found in other lines. This is an interesting case because only $\text{Ly}\alpha$ can be significantly polarized when the main scattering mechanism is Rayleigh. However, their spectral resolution was too insufficient to reveal any polarization structures, which hinders one from drawing a definite conclusion. Future spectropolarimetric observations will shed much light on the AGN unification model.

ACKNOWLEDGEMENTS

We are grateful to the anonymous referees for their useful comments, which improved the presentation of this paper. This research was supported by the Korea Astronomy and Space Science Institute under the R&D program (Project No. 2015-1-320-18) supervised by the Ministry of Science, ICT and Future Planning. This research also received partial support from the Basic Science Research Program through the National Research Foundation (NRF-2014R1A1A2054887). Y.Y. acknowledges the partial support from Basic Science Research Program through the National Research Foundation of Korea (NRF) funded by the Ministry of Science, ICT & Future Planning (NRF-2016R1C1B2007782).

REFERENCES

- Ahn, S. -H., Lee, H.-W., 2015, *Journal of the Korean Astronomical Society*, 48, 195
- Angel, J. R. P., 1969, *ApJ*, 158, 219
- Antonucci, R., 1993, *ARA&A*, 31, 473
- Antonucci, R., Miller, J. S., 1985, *ApJ*, 297, 621
- Bach, K, Lee, H.-W., 2014, *Journal of the Korean Astronomical Society*, 47, 187
- Berestetskii, V. B., Lifshitz, E. M., Pitaevskii, V. B., 1971, *Relativistic quantum theory*(Reading: Pergamon Press)
- Blandford, R. D., Netzer, H., Woltjer, L., Courvoisier, T. J.-L., Mayor, M., 1990, *Active Galactic Nuclei*(Reading: Springer-Verlag)
- Comastri, A., Gilli, R., Marconi, A., Risaliti, G., Salvati, M. 2015, *A&A*, 574, 10
- Comastri, A., Setti, G., Zamorani, G., Hasinger, G., 1995, *A&A*, 296, 1
- Chang, S.-J., Heo, J.-E., Di Mille, F., Angeloni, R., Palma, T., Lee, H.-W., 2015, *ApJ*, 814, 98
- Chandrasekhar, 1960, *Radiative Transfer* (Reading : New York Dover)
- Dey, A., et al. 2005, *ApJ*, 629, 654
- Dijkstra, M., Loeb, A., 2008, *MNRAS*, 386, 492
- Francis, P. J., et al. 2001, *ApJ*, 554, 1001
- Gavril, M., 1967, *PhRv*, 163, 147
- Gilli, R., Comastri, A., Hasinger, G., 2007, *A&A*, 463, 79
- Hayes, M., Scarlata, C., & Siana, B. 2011, *Nature*, 476, 304
- Islaker, H., Nussbaumer, H., Vogel, M., 1989, *A&A*, 219, 271
- Koratkar, A., Antonucci, R. R. J., Goodrich, R. W., Bushouse, H., Kinney, A. L., 1995, *ApJ*, 450, 501
- Lee, H.-W., 2013, *ApJ*, 772, 123
- Lee, H.-W., Blandford, R. D., Western, L., 1994, *MNRAS*, 267, 303
- Lykins, M. L., Ferland, G. J., Kisieli, R., 2015, *ApJ*, 807, 118
- Magdziarz, Pawel, Zdziarski, Andrzej A., 1995, *MNRAS*, 273, 837
- Matsuda, Y., et al. 2004, *AJ*, 128, 569
- Matsuda, Y., Yamada, T., Hayashino, T., et al. 2011, *MNRAS*, 410, L13
- Miller, J. S., Goodrich, R. W., 1993, *PASP*, 355, 456
- Netzer, H., 2015, *ARA&A*, 53, 365
- Nilsson, K. K., Fynbo, J. P. U., Møller, P., Sommer-Larsen, J., & Ledoux, C. 2006, *A&A*, 452, L23
- Peterson, Bradley M., 1993, *PASP*, 105, 247
- Phillips, K. C., Meszaros, P., 1986, *ApJ*, 310, 284
- Prescott, M. K. M., Dey, A., & Jannuzi, B. T. 2012, *ApJ*, 748, 125
- Ricci, C.; Ueda, Y.; Ichikawa, K.; Paltani, S.; Boissay, R.; Gandhi, P.; Stalevski, M.; Awaki, H, 2014, *A&A*, 142, 15
- Sadeghpour, H. R., Dalgarno A., 1992, *JPhB*, 25, 4801
- Saslow, W. M., Mills, D. L., 1969, *PhRv*, 187, 1025
- Schmid, H. M., 1995, *MNRAS*, 275, 227
- Steidel, C. C., Adelberger, K. L., Shapley, A. E., Pettini, M., Dickinson, M., & Giavalisco, M. 2000, *ApJ*, 532, 170
- Totani, T., Aoki, K., Hattori, T., Kawai, N., 2016, *PASJ*, 68, 15
- Tran, H. D., Brotherton, M. S., Stanford, S. A., van Breugel, W., Dey, A., Stern, D., Antonucci, R., 1999, *ApJ*, 516, 85
- Vanden Berk, D. E., Richards, G. T., Bauer, A., 2001, *AJ*, 122, 549
- Yang, Y., Zabludoff, A., Tremonti, C., Eisenstein, D., & Davé, R. 2009, *ApJ*, 693, 1579
- Yang, Y., Zabludoff, A., Eisenstein, D., & Davé, R. 2010, *ApJ*, 719, 1654

This paper has been typeset from a \TeX / \LaTeX file prepared by the author.